Research Article | Vol. 24, No. 15 | 25 Jul 2016 | OPTICS EXPRESS 16586

Optics EXPRESS

Optical constants of $CH_3NH_3PbBr_3$ perovskite thin films measured by spectroscopic ellipsometry

MOHD SHARIZAL ALIAS,[1,4] IBRAHIM DURSUN,[2] MAKHSUD I. SAIDAMINOV,[2] ELHADJ MARWANE DIALLO,[3] PAWAN MISHRA,[1] TIEN KHEE NG,[1] OSMAN M. BAKR,[3] AND BOON S. OOI[1,5]

[1]*Photonics Laboratory, Computer, Electrical, and Mathematical Sciences and Engineering (CEMSE), King Abdullah University of Science & Technology (KAUST), Thuwal, 23955-6900, Saudi Arabia*
[2]*Solar & Photovoltaics Engineering Research Center (SPERC), King Abdullah University of Science & Technology (KAUST), Thuwal, 23955-6900, Saudi Arabia*
[3]*Advanced Nanofabrication Core Lab, King Abdullah University of Science & Technology (KAUST), Thuwal, 23955-6900, Saudi Arabia*
[4]*mohdsharizal.binalias@kaust.edu.sa*
[5]*boon.ooi@kaust.edu.sa*

Abstract: The lack of optical constants information for hybrid perovskite of $CH_3NH_3PbBr_3$ in thin films form can delay the progress of efficient LED or laser demonstration. Here, we report on the optical constants (complex refractive index and dielectric function) of $CH_3NH_3PbBr_3$ perovskite thin films using spectroscopic ellipsometry. Due to the existence of voids, the refractive index of the thin films is around 8% less than the single crystals counterpart. The energy bandgap is around 2.309 eV as obtained from photoluminescence and spectrophotometry spectra, and calculated from the SE analysis. The precise measurement of optical constants will be useful in designing optical devices using $CH_3NH_3PbBr_3$ thin films.

OCIS codes: (300.0300) Spectroscopy; (260.2130) Ellipsometry and polarimetry; (120.4530) Optical constants; (310.6860) Thin films, optical properties.

References and links

1. M. A. Green, A. Ho-Baillie, and H. J. Snaith, "The emergence of perovskite solar cells," Nat. Photonics **8**(7), 506–514 (2014).
2. P. Gao, M. Gratzel, and M. K. Nazeeruddin, "Organohalide lead perovskites for photovoltaic applications," Energy Environ. Sci. **7**(8), 2448–2463 (2014).
3. S. D. Stranks and H. J. Snaith, "Metal-halide perovskites for photovoltaic and light-emitting devices," Nat. Nanotechnol. **10**(5), 391–402 (2015).
4. M. Petrović, V. Chellappan, and S. Ramakrishna, "Perovskites: solar cells & engineering applications – materials and device developments," Sol. Energy **122**, 678–699 (2015).
5. J. Cui, H. Yuan, J. Li, X. Xu, Y. Shen, H. Lin, and M. Wang, "Recent progress in efficient hybrid lead halide perovskite solar cells," Sci. Technol. Adv. Mater. **16**(3), 036004 (2015).
6. Y. Zhao and K. Zhu, "Organic-inorganic hybrid lead halide perovskites for optoelectronic and electronic applications," Chem. Soc. Rev. **45**(3), 655–689 (2016).
7. H. Fujiwara, *Spectroscopic Ellipsometry: Principles and Applications* (John Wiley & Sons, Ltd., 2007).
8. G. Xing, N. Mathews, S. S. Lim, N. Yantara, X. Liu, D. Sabba, M. Grätzel, S. Mhaisalkar, and T. C. Sum, "Low-temperature solution-processed wavelength-tunable perovskites for lasing," Nat. Mater. **13**(5), 476–480 (2014).
9. J. M. Ball, S. D. Stranks, M. T. Horantner, S. Huttner, W. Zhang, E. J. W. Crossland, I. Ramirez, M. Riede, M. B. Johnston, R. H. Friend, and H. J. Snaith, "Optical properties and limiting photocurrent of thin-film perovskite solar cells," Energy Environ. Sci. **8**(2), 602–609 (2015).
10. C.-W. Chen, S.-Y. Hsiao, C.-Y. Chen, H.-W. Kang, Z.-Y. Huang, and H.-W. Lin, "Optical properties of organometal halide perovskite thin films and general device structure design rules for perovskite single and tandem solar cells," J. Mater. Chem. A Mater. Energy Sustain. **3**(17), 9152–9159 (2015).
11. M. A. Green, Y. Jiang, A. M. Soufiani, and A. Ho-Baillie, "Optical properties of photovoltaic organic–inorganic lead halide perovskites," J. Phys. Chem. Lett. **6**(23), 4774–4785 (2015).
12. Y. Jiang, M. A. Green, R. Sheng, and A. Ho-Baillie, "Optical modelling data for room temperature optical properties of organic-inorganic lead halide perovskites," Data Brief **3**, 201–208 (2015).

#264803
Journal © 2016

http://dx.doi.org/10.1364/OE.24.016586
Received 9 May 2016; revised 8 Jul 2016; accepted 10 Jul 2016; published 14 Jul 2016

Optics EXPRESS

13. Q. Lin, A. Armin, R. C. R. Nagiri, P. L. Burn, and P. Meredith, "Electro-optics of perovskite solar cells," Nat. Photonics **9**(2), 106–112 (2015).
14. P. Löper, M. Stuckelberger, B. Niesen, J. Werner, M. Filipič, S.-J. Moon, J.-H. Yum, M. Topič, S. De Wolf, and C. Ballif, "Complex refractive index spectra of $CH_3NH_3PbI_3$ perovskite thin films determined by spectroscopic ellipsometry and spectrophotometry," J. Phys. Chem. Lett. **6**(1), 66–71 (2015).
15. X. Ziang, L. Shifeng, Q. Laixiang, P. Shuping, W. Wei, Y. Yu, Y. Li, C. Zhijian, W. Shufeng, D. Honglin, Y. Minghui, and G. G. Qin, "Refractive index and extinction coefficient of $CH_3NH_3PbI_3$ studied by spectroscopic ellipsometry," Opt. Mater. Express **5**(1), 29–43 (2015).
16. Y. Jiang, A. M. Soufiani, A. Gentle, F. Huang, A. Ho-Baillie, and M. A. Green, "Temperature dependent optical properties of $CH_3NH_3PbI_3$ perovskite by spectroscopic ellipsometry," Appl. Phys. Lett. **108**(6), 061905 (2016).
17. L. J. Phillips, A. M. Rashed, R. E. Treharne, J. Kay, P. Yates, I. Z. Mitrovic, A. Weerakkody, S. Hall, and K. Durose, "Maximizing the optical performance of planar $CH_3NH_3PbI_3$ hybrid perovskite heterojunction stacks," Sol. Energy Mater. Sol. Cells **147**, 327–333 (2016).
18. M. Shirayama, H. Kadowaki, T. Miyadera, T. Sugita, M. Tamakoshi, M. Kato, T. Fujiseki, D. Murata, S. Hara, T. N. Murakami, S. Fujimoto, M. Chikamatsu, and H. Fujiwara, "Optical transitions in hybrid perovskite solar cells: ellipsometry, density functional theory, and quantum efficiency analyses for $CH_3NH_3PbI_3$," Phys. Rev. Appl. **5**(1), 014012 (2016).
19. J.-S. Park, S. Choi, Y. Yan, Y. Yang, J. M. Luther, S.-H. Wei, P. Parilla, and K. Zhu, "Electronic structure and optical properties of α-$CH_3NH_3PbBr_3$ perovskite single crystal," J. Phys. Chem. Lett. **6**(21), 4304–4308 (2015).
20. S. Brittman and E. C. Garnett, "Measuring n and k at the microscale in single crystals of $CH_3NH_3PbBr_3$ perovskite," J. Phys. Chem. C **120**(1), 616–620 (2016).
21. A. M. A. Leguy, P. Azarhoosh, M. I. Alonso, M. Campoy-Quiles, O. J. Weber, J. Yao, D. Bryant, M. T. Weller, J. Nelson, A. Walsh, M. van Schilfgaarde, and P. R. F. Barnes, "Experimental and theoretical optical properties of methylammonium lead halide perovskites," Nanoscale **8**(12), 6317–6327 (2016).
22. Z. K. Tan, R. S. Moghaddam, M. L. Lai, P. Docampo, R. Higler, F. Deschler, M. Price, A. Sadhanala, L. M. Pazos, D. Credgington, F. Hanusch, T. Bein, H. J. Snaith, and R. H. Friend, "Bright light-emitting diodes based on organometal halide perovskite," Nat. Nanotechnol. **9**(9), 687–692 (2014).
23. R. L. Z. Hoye, M. R. Chua, K. P. Musselman, G. Li, M.-L. Lai, Z.-K. Tan, N. C. Greenham, J. L. MacManus-Driscoll, R. H. Friend, and D. Credgington, "Enhanced performance in fluorene-free organometal halide perovskite light-emitting diodes using tunable, low electron affinity oxide electron injectors," Adv. Mater. **27**(8), 1414–1419 (2015).
24. Y.-H. Kim, H. Cho, J. H. Heo, T.-S. Kim, N. Myoung, C.-L. Lee, S. H. Im, and T.-W. Lee, "Multicolored organic/inorganic hybrid perovskite light-emitting diodes," Adv. Mater. **27**(7), 1248–1254 (2015).
25. G. Li, Z.-K. Tan, D. Di, M. L. Lai, L. Jiang, J. H.-W. Lim, R. H. Friend, and N. C. Greenham, "Efficient light-emitting diodes based on nanocrystalline perovskite in a dielectric polymer matrix," Nano Lett. **15**(4), 2640–2644 (2015).
26. A. Sadhanala, S. Ahmad, B. Zhao, N. Giesbrecht, P. M. Pearce, F. Deschler, R. L. Z. Hoye, K. C. Gödel, T. Bein, P. Docampo, S. E. Dutton, M. F. L. De Volder, and R. H. Friend, "Blue-green color tunable solution processable organolead chloride-bromide mixed halide perovskites for optoelectronic applications," Nano Lett. **15**(9), 6095–6101 (2015).
27. Q. Chen, H. Zhou, Z. Hong, S. Luo, H.-S. Duan, H.-H. Wang, Y. Liu, G. Li, and Y. Yang, "Planar heterojunction perovskite solar cells via vapor-assisted solution process," J. Am. Chem. Soc. **136**(2), 622–625 (2014).
28. R. Sheng, A. Ho-Baillie, S. Huang, S. Chen, X. Wen, X. Hao, and M. A. Green, "Methylammonium lead bromide perovskite-based solar cells by vapor-assisted deposition," J. Phys. Chem. C **119**(7), 3545–3549 (2015).
29. G. E. Jellison and F. A. Modine, "Parameterization of the optical functions of amorphous materials in the interband region," Appl. Phys. Lett. **69**(3), 371–373 (1996).
30. S. Kohli, V. Manivannan, J. N. Hilfiker, P. R. McCurdy, R. A. Enzenroth, K. L. Barth, W. P. Smith, R. Luebs, and W. S. Sampath, "Effect of chemical treatment on the optical properties of a cadmium telluride photovoltaic device investigated by spectroscopic ellipsometry," J. Sol. Energy Eng. **131**(2), 021009 (2009).
31. K. Von Rottkay and M. Rubin, "Optical indices of pyrolytic tin-oxide glass," in *MRS Proceedings*, A. Catalano, ed. (MRS, 1996) pp. 449–454.
32. C. Braganza, L. C. Chien, M. R. Fisch, and R. G. Petschek, "Spectrographic ellipsometry study of a liquid crystal display substrate consisting of thin films of SiO_2, polyimide and indium tin oxide on glass," Thin Solid Films **519**(13), 4384–4389 (2011).
33. J. Tauc, R. Grigorovici, and A. Vancu, "Optical properties and electronic structure of amorphous germanium," Phys. Status Solidi, B Basic Res. **15**(2), 627–637 (1966).
34. A. Kojima, K. Teshima, Y. Shirai, and T. Miyasaka, "Organometal halide perovskites as visible-light sensitizers for photovoltaic cells," J. Am. Chem. Soc. **131**(17), 6050–6051 (2009).
35. J. H. Noh, S. H. Im, J. H. Heo, T. N. Mandal, and S. I. Seok, "Chemical management for colorful, efficient, and stable inorganic-organic hybrid nanostructured solar cells," Nano Lett. **13**(4), 1764–1769 (2013).
36. D. A. G. Bruggeman, "Berechnung verschiedener physikalischer Konstanten von heterogenen Substanzen. I. Dielektrizitätskonstanten und Leitfähigkeiten der Mischkörper aus isotropen Substanzen," Ann. Phys. **416**(7), 636–664 (1935).

Optics EXPRESS

37. K. Tanaka, T. Takahashi, T. Ban, T. Kondo, K. Uchida, and N. Miura, "Comparative study on the excitons in lead-halide-based perovskite-type crystals $CH_3NH_3PbBr_3$ $CH_3NH_3PbI_3$," Solid State Commun. **127**(9–10), 619–623 (2003).
38. M. Liu, M. B. Johnston, and H. J. Snaith, "Efficient planar heterojunction perovskite solar cells by vapour deposition," Nature **501**(7467), 395–398 (2013).

1. Introduction

The uniqueness of hybrid perovskites of $CH_3NH_3PbX_3$ (where X is single or a mixture of Cl, Br, or I halides) in term of fabrication ease, large absorption coefficients, high carrier mobility, long carrier diffusion lengths and efficient light-electricity conversion have triggered research phenomena for solar cells recently [1–5]. Combined with additional material properties of high photoluminescence (PL) quantum yield and direct bandgap emission tunability within the visible spectrum, research of this material for other optical devices such as laser, light-emitting diode (LED) and photodetector (PD) are arising [3, 6]. Fundamentally, the information of optical constants whether in the form of an inter-related complex refractive index ($N = n - ik$ where n is the refractive index (RI) and k is the extinction coefficient) or complex dielectric function ($\varepsilon = \varepsilon_1 - i\varepsilon_2$ with $\varepsilon_1 = n^2 - k^2$ and $\varepsilon_2 = 2nk$) as function wavelength or energy are critical. This information will be useful in determining the electronic bandstructure of the perovskite, designing perovskite heterostructure or specific layer for waveguiding or light manipulation in laser, LED or tandem solar cells, and analyzing material properties such as carrier dynamic. To determine the optical constants of material, measurement using spectroscopic ellipsometry (SE), a precise and non-destructive technique for measuring optical properties, is widely used. By measuring the polarization shift from the reflected light off the sample surface and applying an appropriate optical dispersion model, the spectral dependent optical constants of a material can be empirically determined [7].

Numerous studies on optical constants of $CH_3NH_3PbX_3$ perovskites were reported recently [8–21]. However, mostly focused on hybrid perovskites of I and Cl halides (as single or as a mixture of halides). Only a few papers specifically reported the optical constants for the $CH_3NH_3PbBr_3$ perovskite [19–21], however all of these experiments were performed on single crystals. Typically, the optical constants of single crystal or bulk material are higher compared to thin films because of higher material densities and fewer defects from voids and surface inhomogeneity. Recent studies of $CH_3NH_3PbI_3$ perovskites have shown that the RI at 1.55 eV is approximately 2.45 for the single crystal, whereas for the thin films it is considerably lower at around 1.95 [21]. The discrepancy in RI can be detrimental for designing efficient device structures, or light manipulation layers for perovskite optical devices based on thin films. This can lead to poor light confinement, operating wavelength shifting and inefficient light reflection or absorption. Recently, several perovskite LEDs based on $CH_3NH_3PbBr_3$ thin film were reported [22–26], however the absence of optical constant information for this material in thin films form can delay the progress of efficient LED or laser demonstration.

Here, we report a comprehensive study on optical constants (complex RI and complex dielectric function) of $CH_3NH_3PbBr_3$ perovskite thin films deposited on FTO substrate with compact-TiO_2 (c-TiO_2) as an electron transport layer. The analysis is performed at room temperature (RT) using the phase modulated SE technique. The optical constants findings will be very useful for (1) quantifying the RI deviation between the $CH_3NH_3PbBr_3$ perovskite thin films and single crystals, (2) improving the $CH_3NH_3PbBr_3$ perovskite thin films fabrication, and (3) designing heterostructure for $CH_3NH_3PbBr_3$ perovskite-based laser, LED, PD and tandem solar cell devices. For these devices, the perovskite deposition using thin films approach is more relevant to form a thin multilayer structure.

Optics EXPRESS

2. Experiment

2.1 $CH_3NH_3PbBr_3$ thin films deposition and characterization

$CH_3NH_3PbX_3$ perovskites thin films can be fabricated using techniques of one-step precursor deposition (OSPD), sequential deposition method (SDM), dual-source vapor deposition (DSVD) and vapor assisted solution process (VASP). The details of fabrication steps and the advantages plus limitations for each technique are reviewed elsewhere [2, 4]. In this work, the $CH_3NH_3PbBr_3$ thin films were deposited using VASP method [27, 28]. This technique allows uniform films thickness, extensive films coverage and small surface roughness for the formation of high-quality perovskites thin films suited for multilayer devices. Initially, the FTO substrate was ultrasonically cleaned in detergent, DI water, acetone and IPA, then blow dried by N_2 and treated with O_2 plasma. Prior to $CH_3NH_3PbBr_3$ films deposition, the FTO substrate was spin coated with approximately 40 nm thickness of c-TiO_2 using mildly acidic titanium isopropoxide solution and heated at 500 °C for 15 min to smoothen the surface and to mimic as the electron transport layer deployed in mostly solar cells and LED devices. The 0.8M $PbBr_2$ solution in DMF was then spin coated and annealed at 100 °C for 10 min. After annealing, the films was treated by CH_3NH_3Br vapor at 145 °C for 1 hours in a closed petri dish with CH_3NH_3Br powder surrounding the substrate on a hot plate in a vacuum chamber and then rinsed with IPA.

Powder X-ray diffraction (XRD) for the deposited thin films was performed using Bruker AXS D8 diffractometer with Cu-K_α radiation. Surface roughness analysis were performed using Agilent Technologies 5400 atomic force microscope (AFM) under tapping mode operation for an area of 2.5×2.5 and 5×5 μm^2. The surface and cross-section microscopies were performed using FEI Quanta 3DFEG scanning electron microscope (SEM). The RT PL spectra were acquired using a Horiba Jobin Yvon Aramis UV spectrometer with a 473-nm excitation laser. All reflectance and transmittance spectra were measured with a Shimadzu UV3600 spectrophotometer equipped with integrating sphere and baselined to Al mirror.

2.2 Spectroscopic ellipsometry measurement

The SE measurement was performed using a phase modulated SE (Horiba Jobin Yvon UVISEL iHR320) at RT. Typically, SE data is measured in the form of ellipsometric angles of Ψ and Δ as a function of energy. However, for the phase modulated SE, the detected signals are in the form of the first and second harmonics (symbolized as I_S and I_C) of the base modulation frequency of the polarized light upon reflection and can be extracted to determine Ψ and Δ parameters [7, 14]. Measurements were performed at incident angles of 60, 65 and 70° for a spectral range between 1.5 to 5 eV with a 0.05 eV sampling step. The analysis of the SE data was performed using Horiba Jobin Yvon DeltaPsi2 software.

2.3 Optical dispersion model

After SE measurement, optical model fitting using appropriate dispersion model is performed to extract the optical constants, films thickness and surface morphology. A good fit to the measured data indicated by lowest mean squared error (MSE) is required across the entire spectral range. The Levenberg-Marquardt regression algorithm [7] was used for minimizing the MSE. We utilized Tauc-Lorentz (T-L) model [29], Drude-Lorentz (D-L) model [7], and New Amorphous model [14], for the $CH_3NH_3PbBr_3$ perovskite thin films, FTO substrate, and c-TiO_2 respectively. Except for the New Amorphous model, all of these models are Kramers-Kronig consistent. We applied T-L model since the similar model was used in the optical constant study of $CH_3NH_3PbBr_3$ single crystal [19], thus any deviation in our results can be assumed due to the sample (thin films versus crystal) and not owing to the disparity in SE modelling approach. The D-L dispersion model is commonly used for transparent conductive oxide films such as ITO and FTO [30–32].

Optics EXPRESS

2.4 Absorption coefficient spectra

The absorption coefficient (α) spectra is calculated using equation of $\alpha = 4\pi k/\lambda$ where λ is the wavelength and k is derived from the SE measurement. In addition to the PL and spectrophotometry measurements, the energy bandgap (E_g), is also calculated using the Tauc plot [33] of $(\alpha E) = A\left(E - E_g\right)^{1/2}$ where α is the absorption coefficient, E is energy, and A is a constant. The E_g value is acquired by extrapolating the linear fit line back to the x-axis $(\alpha E = 0)$.

3. Results and discussion

Material characterizations for the $CH_3NH_3PbBr_3$ perovskite thin films were performed to analyze the structural, morphology and optical properties. The XRD spectra shown in Fig. 1(a) verified the formation of the $CH_3NH_3PbBr_3$ films on the FTO/c-TiO_2 substrate. The peaks of the $CH_3NH_3PbBr_3$, c-TiO_2 and FTO were found consistent with the literature [34, 35]. The SEM and AFM microscopies indicate films morphology with grain sizes of 100-850 nm in diameter and vertical root-mean-square roughness (RMS) of 37.0 nm (Fig. 1(b) and the inset). The PL spectra shown in Fig. 1(c) exhibits E_g around 537 nm. The spectrophotometry spectra (Fig. 1(d)) indicate absorptance at wavelengths below the absorption edge (<537 nm).

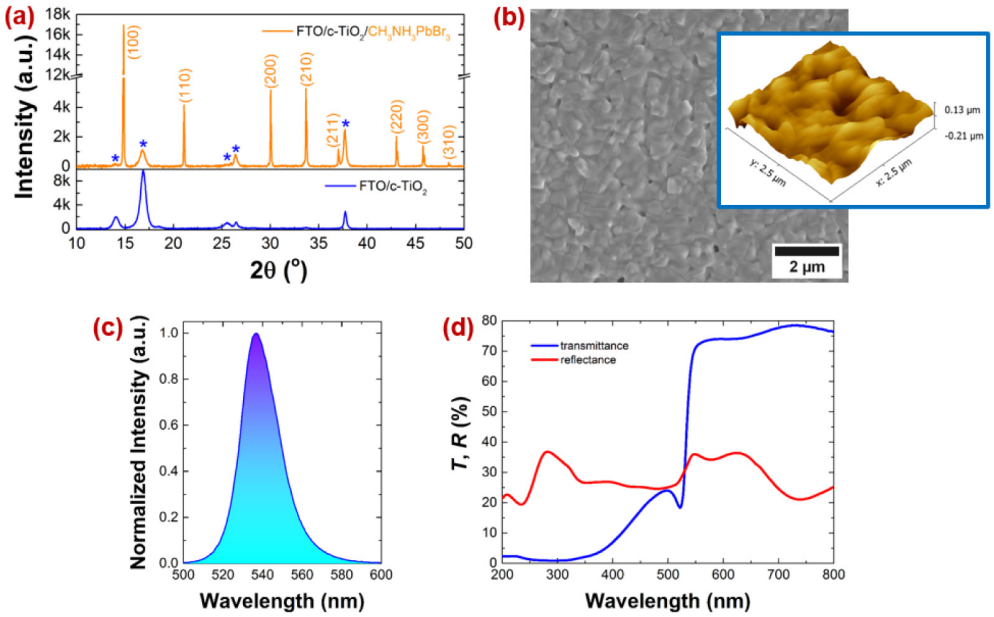

Fig. 1. Material characterizations of $CH_3NH_3PbBr_3$ perovskite thin films deposited on FTO with c-TiO_2 buffering showing: (a) XRD spectra, (b) SEM top-view with 3D AFM topography inset, (c) PL spectra, and (d) spectrophotometry spectra.

Due to the complexity of multilayer structure in our sample ($CH_3NH_3PbBr_3$ thin films/c-TiO_2 buffer layer/FTO substrate) plus the FTO substrate itself composed of 3 layers (typically 340 nm SnO_2:F, 25 nm SiO_2 and 30 nm SnO_2 layers coated on 2 mm glass [9]), we initially performed SE measurement for the bare substrate (glass pre-coated FTO). With this approach, we decoupled the complexity of the SE fitting which can arise from the multilayer interference during the measurement and coupling of optical model parameters during the SE modelling. This resulted in a good fitting agreement for the full sample analysis (shown later).

Optics EXPRESS

Figure 2(a) shows the SE measured versus modelled spectra for the FTO substrate with good fitting acquired (MSE of 1.66) for the entire spectral range. The optical stack model shown in Fig. 2(b) represents the FTO substrate used for the SE modelling. Figure 2(c) depicts the extracted optical constants of n and k for the FTO substrate as a function of wavelength. The thickness of 429.5 nm and RMS of 18.0 nm (using effective medium approximation (EMA) of 55% SnO_2:F and 45% voids based on the Bruggeman theory [36]) obtained from the modelled FTO substrate are in good agreement with the measured SEM cross-section (425.7 nm) and RMS from AFM (18.7 nm) shown in Figs. 2(d) and 2(e), respectively. Additionally, we also performed SE measurement for the c-TiO_2 layer (spin coated on the bare FTO substrate). Figure 2(f) shows the extracted optical constants of n and k for the c-TiO_2 layer.

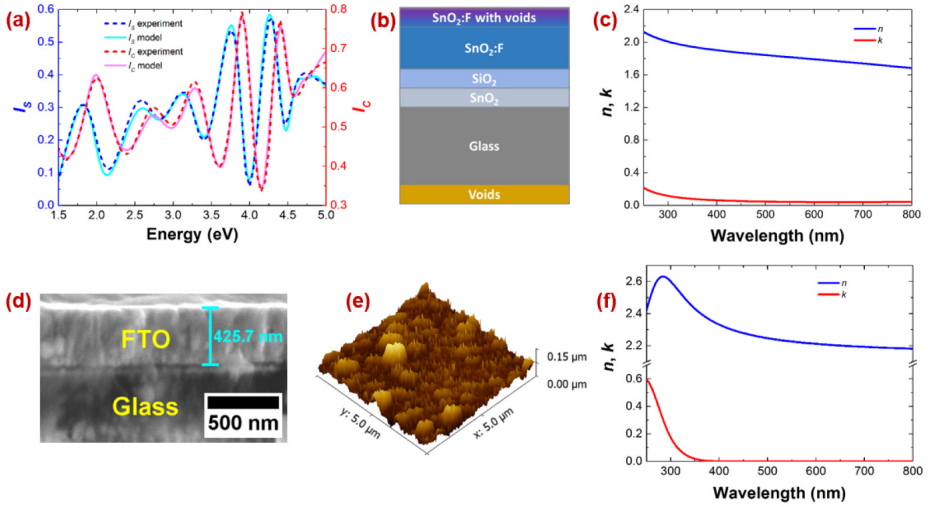

Fig. 2. Measurement and analysis for the FTO substrate showing: (a) fitting of measured and modelled SE spectra with MSE of 1.66, (b) schematic of the optical model, (c) wavelength-dependent optical constants, (d) cross-section SEM, and (e) 3D AFM topography. Measurement of SE is also conducted for c-TiO_2 layer to determine the wavelength-dependent optical constants, as shown in (f).

Figure 3(a) shows the SE measured versus modelled spectra for the full sample comprised of $CH_3NH_3PbBr_3$ perovskite thin films coated on the glass pre-coated FTO substrate with a c-TiO_2 buffer in between. The spectra exhibit a good agreement across the entire spectral range. We obtained an MSE of approximately 1.54 (typically MSE <10 for a film with thickness >500 nm). From the spectra, several peaks were observed above the absorption edge (>2.31 eV) located at approximately 2.36, 3.58 and 4.55 eV. These peak points are consistent with previously reported spectra [19, 37]. To accommodate these peak points, the T-L model fit for the $CH_3NH_3PbBr_3$ perovskite thin films requires three oscillators. We also acquired reasonable spectral fitting for SE measurement at various angles of incidence (MSE of 1.94 for 65° and 2.17 for 60°, respectively), however we only show here for the best MSE obtained from the 70° incidence angle measurement. To minimize the MSE from the SE modelling, the films thickness and surface roughness of $CH_3NH_3PbBr_3$ perovskite thin films were treated as free fitting parameters whereas the thickness and surface roughness of the FTO substrate and c-TiO_2 layer were fixed using values obtained from the above SE analysis. The optical stack model deployed for this full sample SE analysis is shown in Fig. 3(b). For the $CH_3NH_3PbBr_3$ perovskite thin films, we employed two layers to model the main layer and the surface roughness. Besides voids consideration on the surface layer, we also considered voids presence in the main layer to reflect pin-holes existence. The modelled thickness for $CH_3NH_3PbBr_3$ perovskite thin films and c-TiO_2 layer are highly accurate (less than 4% and

Optics EXPRESS

10% deviations for the former and latter layers, respectively) in comparison with the SEM cross-section shown in Fig. 3(c). The modelled RMS of 33.5 nm with EMA of 84% $CH_3NH_3PbBr_3$ films and 16% voids for the surface layer is also in good agreement with the previously measured AFM (RMS of 37.0 nm in Fig. 1(b)). The SE modelling also indicated approximately 5% of voids exist (from pin-holes) in the main layer of the $CH_3NH_3PbBr_3$ perovskite thin films.

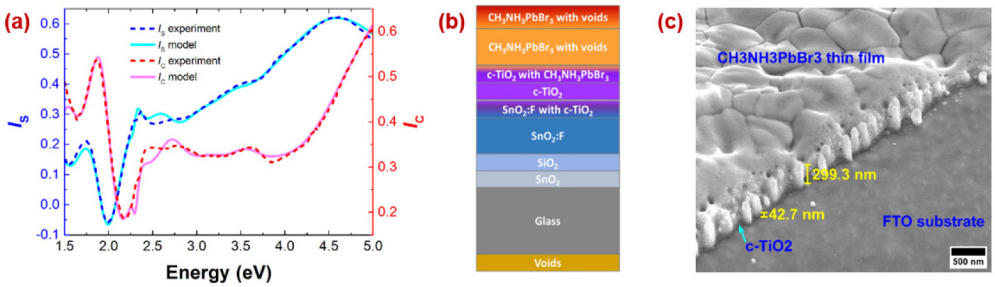

Fig. 3. Measurement and analysis of $CH_3NH_3PbBr_3$ perovskite thin films on glass pre-coated with FTO and a c-TiO_2 buffer layer showing (a) fitting of measured and modelled SE spectra with MSE of 1.54, (b) schematic of the optical model, and (c) angled SEM cross-section view (tilted at 52°) indicating the $CH_3NH_3PbBr_3$ films, c-TiO_2 buffer layer and FTO substrate.

Figure 4(a) shows the extracted optical constants of n and k of $CH_3NH_3PbBr_3$ perovskite thin films as a function of wavelength. For comparison, we plotted the RI spectra of reported $CH_3NH_3PbBr_3$ perovskite single crystals using SE measurement with T-L model [19], SE measurement with a critical points-joint density of state model [21], and using spectrophotometry with nonlinear regression model [20]. It is observed that the RI of $CH_3NH_3PbBr_3$ perovskite thin films is lower than all single crystals counterpart. At 535 nm wavelength for example (Fig. 4(b)), the RI of $CH_3NH_3PbBr_3$ thin films is around 2.29 whereas all single crystals exhibit 2-8% higher RI. Higher RI of around 25% is also observed for the $CH_3NH_3PbI_3$ perovskite single crystals case compared to the equivalent thin films [21]. The disparities of RI values between all perovskite thin films and single crystals can induce weak guiding of light when designing heterostructure devices such as laser, LED and tandem solar cells. Moreover, if the heterostructure is based on perovskite with different halides (such as a combination of $CH_3NH_3PbI_3$/$CH_3NH_3PbBr_3$), the precise values of RI will become more crucial since the RI range is within proximity to each other. Figure 4(c) shows the dielectric functions of the $CH_3NH_3PbBr_3$ perovskite thin films. We obtained approximately 5.1 for the dielectric function near the absorption edge which is close to the reported value of 4.8 measured using spectrophotometry [37]. As for the k and ε_2 spectra, the absorption edge of around 2.309 eV is consistent with most reported values for $CH_3NH_3PbBr_3$ perovskite [11, 19, 21, 28]. Figure 4(d) shows the absorption coefficient spectra for the $CH_3NH_3PbBr_3$ perovskite thin films plotted together with the spectra of single crystals [19] for comparison. Both spectra exhibit almost similar absorption edges and peak positions. Using the Tauc plot (inset of Fig. 4(d)), the calculated E_g of the $CH_3NH_3PbBr_3$ perovskite thin films is approximately 2.309 eV which is consistent with the PL emission wavelength (Fig. 1(c)) and absorption edge indicated using spectrophotometry (Fig. 1(d)). Although the Tauc plot from SE analysis exhibits good agreement with the PL and spectrophotometry measurements, careful consideration should be applied here because the calculated E_g could be imprecise [11] due to the excitonic effects near the band edge for hybrid perovskites [20].

Optics EXPRESS

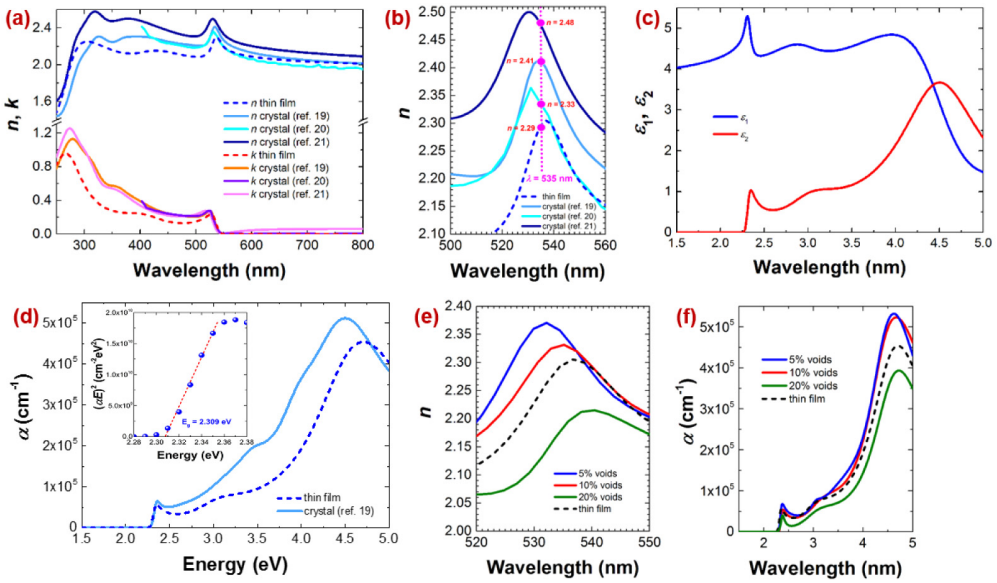

Fig. 4. Spectra of $CH_3NH_3PbBr_3$ perovskite thin films showing (a) wavelength-dependent optical constants and comparison with single crystals, (b) comparison of RI values at specific wavelength for thin films and single crystals, (c) dielectric functions, (d) absorption coefficient and comparison with single crystals (inset showing the Tauc plot), (e) effect of voids on the RI spectra, and (f) effect of voids on the absorption spectra.

The discrepancies of 2-8% in RI (refer Fig. 4(b)) and around one magnitude order in absorption coefficient (refer Fig. 4(d)) between $CH_3NH_3PbBr_3$ perovskite thin films and single crystals can be attributed to the dissimilarities of material densities (due to voids) and surface condition (roughness and homogeneity). It is well-known that perovskite thin films exhibit higher voids compared to single crystals since solution processing involved in most of the perovskite thin films deposition methods normally exhibit pin-holes [2, 4]. These voids can reduce the quality of the material, thus lowering the RI value as shown for $CH_3NH_3PbI_3$ perovskite case with voids included [11].To establish this argument for the $CH_3NH_3PbBr_3$ perovskite thin films, we modelled voids at the film's surface. The voids were varied at 5, 10 and 20% at the surface using the EMA between $CH_3NH_3PbBr_3$ films and air. As for the main $CH_3NH_3PbBr_3$ perovskite layer, we used EMA of 95% $CH_3NH_3PbBr_3$ films and 5% voids as obtained for the best-fit SE spectra (MSE of 1.54 as shown in Fig. 3(a)). From various SEM cross-sections performed (results not shown here), we found that the voids (pin-holes effects) appeared mostly on the sample surface. Figures 4(e) and 4(f) show the increment of RI and absorption coefficient spectra, respectively as the percentage of voids decreased. The excitonic peaks of both spectra were also blue-shifted as the voids diminished. We also plotted the RI and absorption coefficient spectra from the actual sample measurement (dashed lines) for comparison. Although the DSVD deposition method [38] is claiming non-existence of pin-holes for perovskite thin films, substantial voids are still observable between the polycrystalline grains. Thus the voids existence could not be totally omitted in any of the existing thin films deposition methods (OSPD, SDM, DSVD or VASP) which are preferred for the fabrication of multistructure perovskite. Beside voids, other possible factors for the variance of RI can be attributed to the non-stoichiometry of the fabricated samples, mixture of crystalline and amorphous phases in the sample, scattering effect from the randomness of perovskite polycrystals in the thin films, accuracy in measurement method (such as SE modelling and SE versus spectrophotometry), and sample degradation over time.

Optics EXPRESS

4. Conclusion

In our study, we reported comprehensive optical constants and dielectric functions for $CH_3NH_3PbBr_3$ perovskite thin films using SE technique. We found that the RI of the thin films is around 8% less than the single crystals counterpart. We obtained approximately 5.1 for the dielectric function near the absorption edge for the $CH_3NH_3PbBr_3$ perovskite thin films. The E_g is around 2.309 eV as measured using the PL and spectrophotometry techniques, and calculated from the SE measurement. The lower RI observed for the $CH_3NH_3PbBr_3$ perovskite thin films compared to the single crystals counterpart signifies the importance of having precise optical constants database for thin films devices. This is because most of the perovskite based laser, LED, PD and tandem solar cells are relying on the thin films deposition approach in fabricating the heterostructure and multijunction structure. The knowledge of the optical constants will also help to quantify the RI deviation between thin films and single crystal, and improve the fabrications of $CH_3NH_3PbBr_3$ perovskite thin films.

Funding and Acknowledgments

King Abdulaziz City for Science and Technology (KACST) (KACST TIC R2-FP-008); King Abdullah University of Science and Technology (KAUST) (BAS/1/1614-01-01).